ELECTRONIC SUPPLEMENTARY INFORMATION

Harnessing Magnetic Dipole Resonance in Novel Dielectric Nanomaterials

Haobijam Johnson Singh[a,*] and Ambarish Ghosh[a,b,c,**]

[a] Department of Physics, Indian Institute of Science, Bangalore, 560012, India
[b] Centre for Nano Science and Engineering, Indian Institute of Science, Bangalore, 560012, India

[c] Department of Electrical Communications Engineering, Indian Institute of Science, Bangalore 560012, India

* johnsonthonga196@gmail.com

** ambarish@iisc.ac.in

I. Methods Section:

1. Sample Fabrication:

Fabrication of core-shell nanopillar consists of four steps. First a 2D square array of pattern photoresist (PR) is fabricated on a glass substrate using laser interference lithography technique[1]. The patterned PR film was then taken in a Glancing angle deposition (GLAD)[2] chamber and a thin layer (~ 50 nm) of MgF_2 was deposited which acts as a mask for the PR blobs while the residue PR film is exposed. O_2 plasma etching results in nanopillars of PR. Finally the film sample containing PR pillars was then placed in a PECVD[3] (plasma enhanced chemical vapour deposition) chamber for amorphous silicon (a-Si) deposition.

Laser Interference Lithography (LIL)[1]: We used LIL (Laser Interference Lithography) in Lloyd's mirror configuration where a 356 nm laser line was used to create a 2D square array pattern. This was subsequently used as a seed layer for GLAD. The substrates (glass slides) are first cleaned chemically with piranha solution (mixture of H_2SO_4 and H_2O_2 in 3:1 ratio) to remove native oxide and then dehydrated at 250°C on a hot plate for 10 mins to remove any moisture content on the substrates. Once the substrates are cooled downed to room temperature a layer of positive photoresist (PR) (Shipley, 1805) is spin coated at 4000 rpm for about 40 seconds giving a film thickness of about 400 nm. The PR coated substrates are then prebake at 110°C on a hot plate for about a minute. Following this the substrates are exposed under the LIL (laser interference lithography) set up with an average dose of 300 mJ/cm^2 and later developed in MF26A developer (AZ EM electronics). Double exposure technique with 90° substrate rotation was adopted which resulted in 2D square array patterns.

Glancing Angle Deposition (GLAD)[2]: The LIL pattern substrate was used as a seed layer during the deposition of dielectric material which is carried out in a physical vapour deposition chamber equipped with an e-beam source. The pattern glass substrate was placed at an extreme angle (≥ 84°) to the source of incoming vapour and was rotated continuously a speed of 0.15 – 0.3 rpm for MgF_2 deposition. The deposition rate was maintained around 0.2 – 0.3 nm/second and the pressure was less than 6 x10^{-6} mbar.

Plasma Etching: The etching of the MgF_2 deposited PR films were carried out in an ICP-RIE chamber (inductively coupled plasma-reactive ion etching, *Oxford Instruments*) using oxygen plasma. The chamber

pressure was maintained at 10 mtorr and the oxygen flow rate was 10 sccm and the plasma frequency was maintained at 13 MHz.

Plasma Enhanced Chemical Vapor Deposition (PECVD)[3]*:* The film samples containing PR pillars were then placed in a PECVD chamber for amorphous silicon (a-Si) deposition. A mixture of silane, SiH_4, N_2O and Ar gases were used for a-Si deposition which was carried out at 140°C and 1000 mT pressure. This resulted in a conformal coating of a-Si all over the PR pillars (as well as in between the pillars) resulting in a core-shell nanopillar geometry.

2. *Characterization:*

Transmittance: The transmittance measurement of the core-shell dielectric nanoparticle array systems were carried out using an optical fiber based UV-VIS spectrometer (Ocean Optics USB 4000). The light beam emitted from the fibre was first collimated which was then polarised after passing through a Glan-Taylor polarizer. The polarised light was then allowed to incident on the sample normally. The transmitted light was then collecting using a collecting lens and integrated for 30 ms and then finally sent to the USB spectrometer. A glass substrate spin coated with photoresist was used as the reference sample. For near mid IR range UV-VIS-IR spectrometer MPC3600 (Shimadzu) was used.

Ellipsometry: Ellipsometry measurements were carried out using Woollam Ellipsometer equipped with Deuterium and Quartz Tungsten Halogen lamp capable of scanning from 245 nm all the way to 1000 nm wavelength. A thin film of PECVD a-Si deposited both on cleaned silicon wafer as well cleaned glass slide were used for the measurements.

II. Numerical Simulations:

Numerical simulations were carried out using Comsol Multiphysics 5[4], a FEM (finite element method) based numerical software to calculate the optical response of the core-shell nanopillars. We adopted full field formalism with periodic boundary conditions (Floquet) applied on all the four sides of the computational geometry assuming an infinite 2D periodic structure in the x-y plane. The incident beam was assumed to be linearly polarised (LP) along x axis propagating along the long axis (z direction) of the core shell nanopillar. The core-shell nanostructures were positioned at the centre of the computational window without a semi-infinite substrate and assumed to be embedded in air medium ($\varepsilon_m = 1.0$). The frequency dependent complex dielectric function values for silicon used in the simulations were experimentally (ellipsometry) determined. Direct solver method was adopted to solve for the wave equation for LP incident light and the transmittance was extracted using S-parameters which were further used for calculating the transmittance. Sweep parameter was used to scan the wavelength range from 500 nm to 1200 nm.

For calculating single particle response scattered field formalism was adopted. We used a spherical PML of thickness 200 nm and order 1 surrounding the model geometry. The PML was placed at half-wavelength away from the nanopillars. The entire structure was divided into domains and sub-domains, and each domain was meshed using free tetrahedral meshing of maximum element size 6 elements per wavelength outside the dielectric nanoparticle. We adopt iterative solver to solve the wave equation, such as to calculate the extinction cross sections for LP incident lights. Sweep parameter was used to scan the wavelength range from 400 nm to 1200 nm.

Simulation Parameters:

For the results shown in Figure 1B and 1C of the main manuscript and S1 of the supplementary information:

core diameter, d = 100 nm; pillar height, h = 150 nm; shell thicknesses, t = 75 nm and 15 nm

For the results shown in Figure 2S of the supplementary information:

core diameter, d = 100 nm; pillar height, h = 150 nm; shell thicknesses, t = 75 nm

For the results shown in Figure 3S of the supplementary information:

core diameter, d = 100 nm; pillar height, h = 150 nm; shell thicknesses, t = 90 nm, 75 nm, 60 nm, 30 nm, 15 nm, 7.5 nm and 5 nm.

III. Multipole Decomposition:

To analyse the different resonant modes excited in the core-shell nanopillar system multipole decomposition approach described in[5-7] was adopted. For nanoparticle array systems embedded in some medium (e.g. air) multipoles can be computed through the polarization currents induced inside them.

$J = -i\omega\varepsilon_o(\varepsilon - 1)E$

where **E** is the electric field inside the particle, ε and ε_o are the particle permittivity and the free space permittivity respectively. The dipole moments and quadrupole moments induced in the system can be calculated as:

$$electric\ dipole\ moment, p = \int \varepsilon_o(\varepsilon - 1)E\ dV$$

$$magnetic\ dipole\ moment, m = \frac{-i\omega}{2}\int \varepsilon_o(\varepsilon - 1)(r\ x\ E)\ dV$$

$$electric\ quadrupole\ moment, \bar{Q}_e = \frac{1}{2}\int \varepsilon_o(\varepsilon - 1)\left[r \otimes E + E \otimes r - \frac{1}{2}(r.E)\bar{\bar{I}}\right]dV$$

$$magnetic\ quadrupole\ moment, \bar{\bar{Q}}_m = \frac{-i\omega}{3}\int \varepsilon_o(\varepsilon - 1)[r \otimes (r \otimes E) + (r \otimes E) \otimes r]dV$$

where $\otimes$ is the dyadic product and *dV* is the integral over the particle volume.

The scattering cross sections can calculated from the power radiated by the dipoles after normalising by the incident power as:

$$\sigma_{sca}^{ED} = \frac{k_o^4}{6\pi\varepsilon_o^2 E_o^2}\|p\|^2$$

$$\sigma_{sca}^{MD} = \frac{\mu_o k_o^4}{6\pi\varepsilon_o E_o^2}\|m\|^2$$

$$\sigma_{sca}^{EQ} \approx \frac{k_o^6}{80\pi\varepsilon_o^2 E_o^2}\left\|\bar{\bar{Q}}_e\right\|^2$$

$$\sigma_{sca}^{EQ} \approx \frac{\mu_o k_o^6}{80\pi\varepsilon_o E_o^2}\left\|\bar{\bar{Q}}_m\right\|^2$$

where E_o is the incident field amplitude and μ_o is the free space permeability. The contributions of various modes to the scattering cross section goes as modulus square of their respective moments. For simplicity the contributions due to toroidal components[5, 6] are not considered in these calculations.

Supplementary Figures:

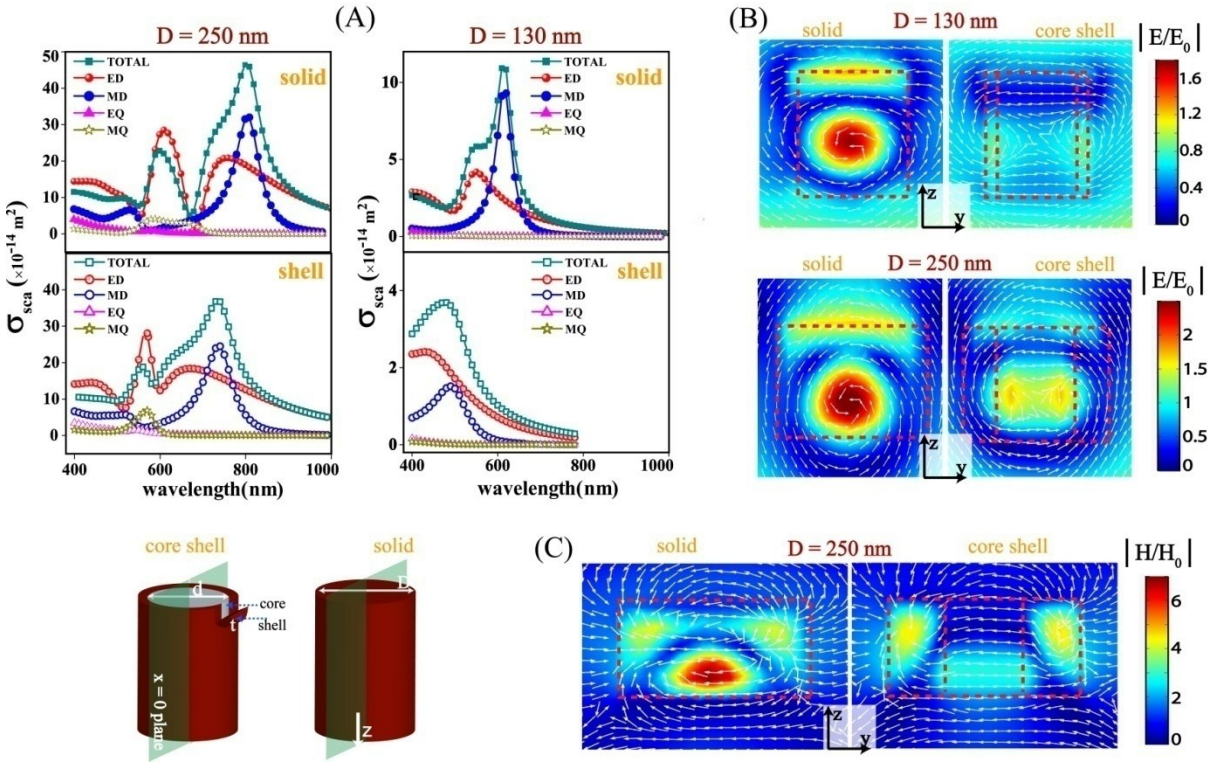

Figure S1: (A) Total scattering cross section along with separate contributions from electric dipoles (ED), magnetic dipoles (MD), electric (EQ) and magnetic quadrupoles (MQ) as calculated through multiple decomposition for solid as well as core-shell geometry (see schematic below; the core is assumed to be SiO_2 and the shell material is a-Si) corresponding to D = 250 nm (75 nm shell thickness) and D = 130 nm (15 nm shell thickness). (B) False colour plot of the norm of electric field enhancement ($|\mathbf{E}/\mathbf{E_0}|$) at x = 0 plane (see schematic) of the core-shell as well as solid nanopillars corresponding to electric dipole modes (ED) at the resonance wavelength for D = 250 nm (75 nm shell thickness) and D = 130 nm (15 nm shell thickness). Arrows (white colour) indicate direction of H vector. Circular distribution of **H** vector in yz plane within the particle confirms the electric dipolar nature of these resonances. (C) False colour plot of the norm of magnetic field enhancement ($|\mathbf{H}/\mathbf{H_0}|$) at x = 0 plane (see schematic) of the core-shell as well as solid nanopillars corresponding to magnetic quadrupole mode (MQ) at the resonance wavelength for D = 250 nm (75 nm shell thickness). Arrows (white colour) indicate direction of E vector in the yz plane.

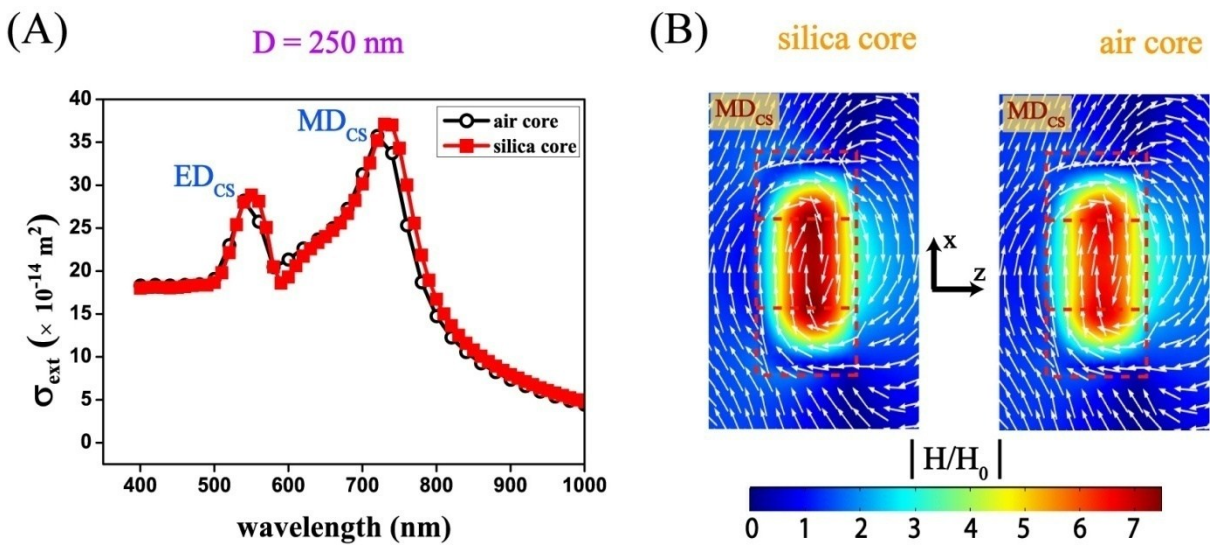

Figure S2: (A) Simulated total extinction cross section of core-shell geometry for air and silica core (shell is aSi) corresponding to D = 250 nm (75 nm shell thickness) (B) Corresponding false colour plot of the norm of magnetic field enhancement ($|\mathbf{H/H_0}|$) at y = 0 plane. As seen a significant amount of magnetic field enhancement still persist inside the shell even in the absence of any core material (air).

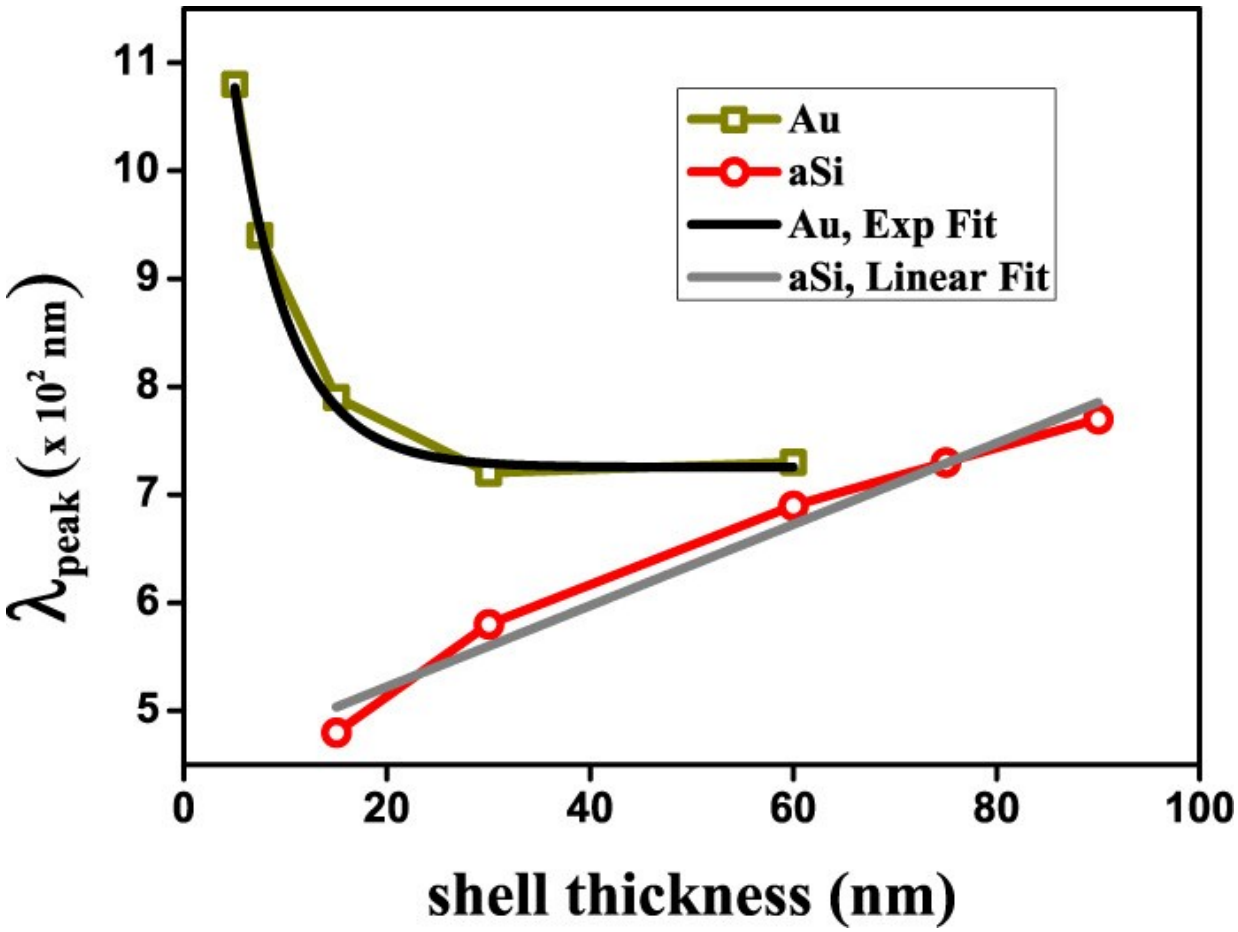

Figure S3: Plot of wavelength corresponding to peak in extinction spectra denoted by λ_{peak}, as a function of shell thickness (core is SiO_2 and diameter is fixed) for Au and a-Si core shell nanopillars. For Au, λ_{peak} corresponds to the bonding mode while for a-Si it corresponds to the magnetic resonance mode. For plasmonic core shell case λ_{peak} follows an exponential decrease with the shell thickness while for dielectrics, it increases linearly.

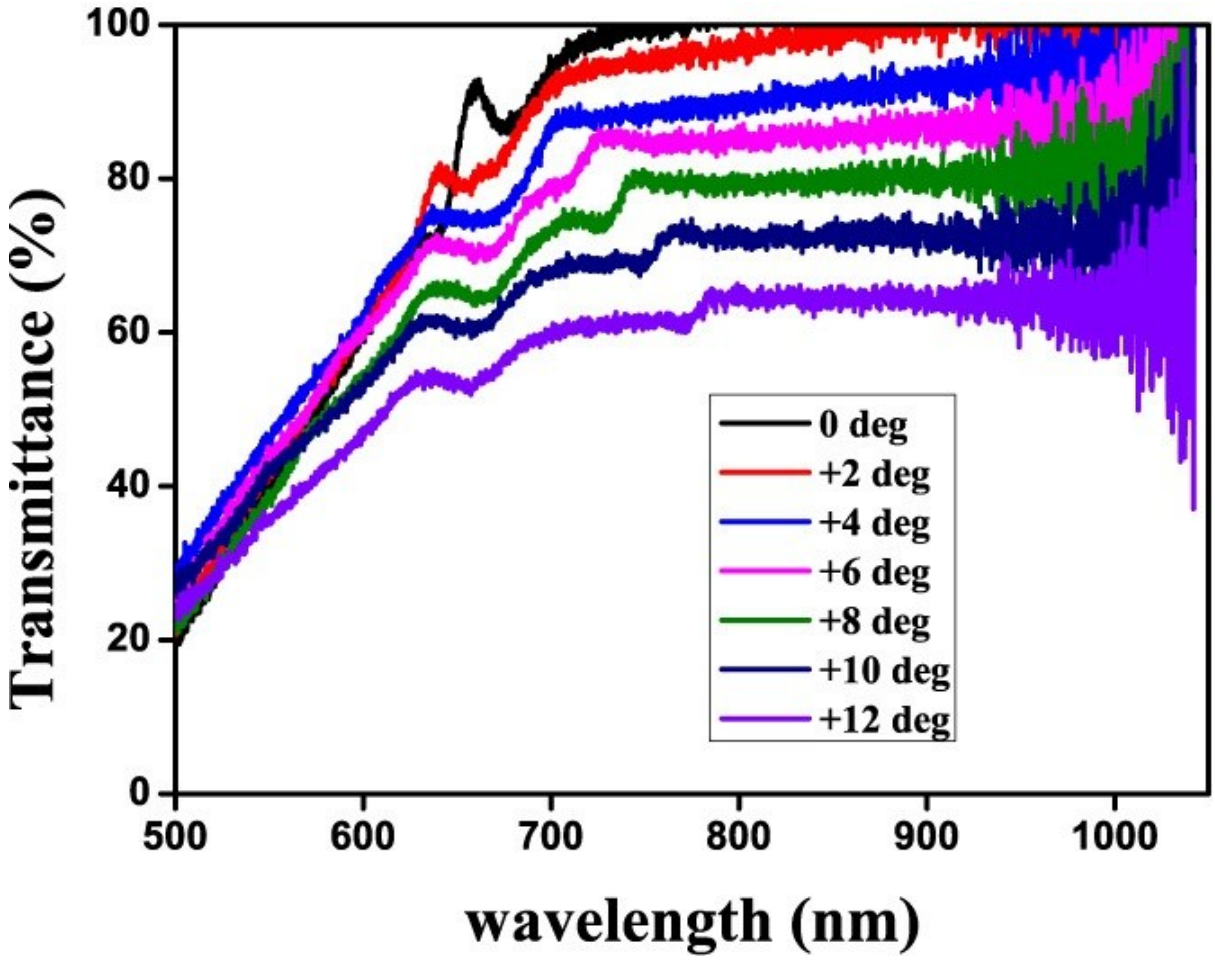

Figure S4: Measured transmittance spectra for patterned PR films as a function of light incident angle.

Schematics of the experimental system:

While the proposed experimental geometry in the current work is of core-shell nanopillars and our fabrication techniques indeed ensures it, SEM image (see Figure 2D of the main manuscript) after PECVD deposition revealed most of the a-Si deposition happens at the top part of the PR pillar even though deposition indeed happen in the lower part of the PR. Keeping this in mind we have model our experimental system like as shown below for numerical calculations where 0.5H (H is the total PR height plus MgF_2 thickness) is assumed to be covered by a-Si while the lower PR part is exposed.

h_1 = height of the PR pillar; h_2 = thickness of MgF_2; h_3 = thickness of a-Si on top

h_4 = total height of a-Si covering the PR pillar (including MgF_2) = $h_3 + (h_1 + h_2)/2$.

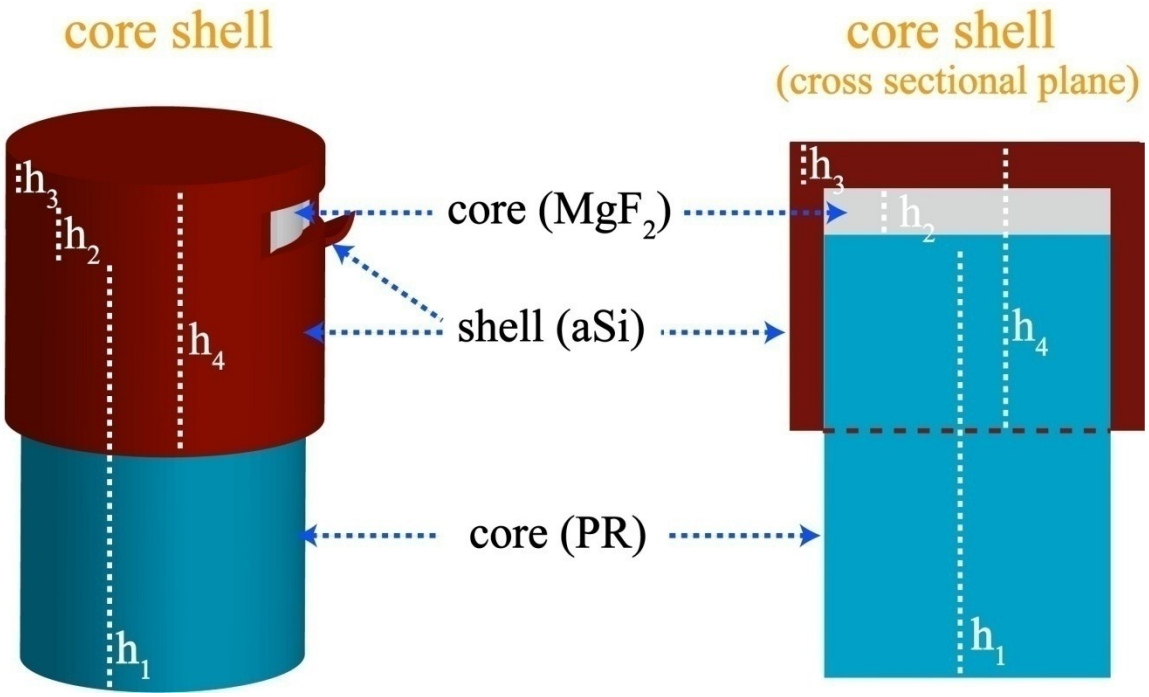

Figure S5: Schematic of the experimental system used in numerical calculations.

Simulation Parameters:
For the results shown in Figure 3C and 3D of the main manuscript and S7 of the supplementary information:

PR core diameter, d = 200 nm; PR pillar height, h_1 = 400 nm; MgF_2 core diameter, d = 200 nm; MgF_2 pillar height, h_2 = 50 nm; Interpillar spacing = 580 nm.

Shell thickness (nm)	h_3 (nm)
15	**30**
23	**45**
30	**60**
38	**75**
45	**90**

For the results shown in Figure S7 of the supplementary information:

580 nm interpillar spacing: PR core diameter, d = 200 nm; PR pillar height, h_1 = 400 nm; MgF_2 core diameter, d = 200 nm; MgF_2 pillar height, h_2 = 50 nm; shell thickness , t =45 nm, h_3 = 90 nm.

1 µm interpillar spacing: PR core diameter, d = 450 nm; PR pillar height, h_1 = 400 nm; MgF_2 core diameter, d = 450 nm; MgF_2 pillar height, h_2 = 50 nm; shell thickness , t =45 nm, h_3 = 90 nm.

For the results shown in Figure S8 of the supplementary information:

film thickness = 38 nm, array periodicity = 580 nm, largest hole size = 200 nm

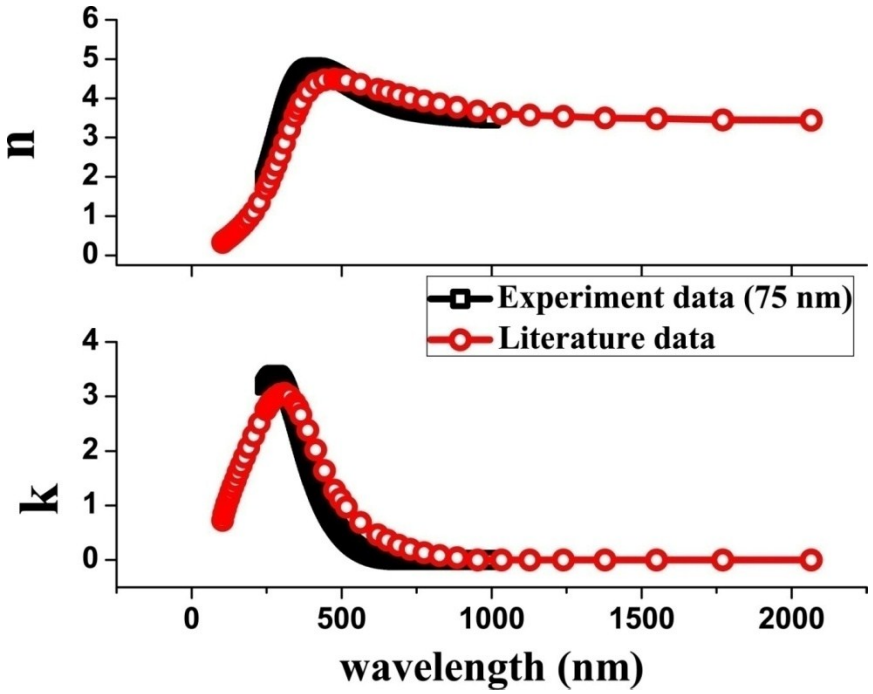

Figure S6: Experimentally determined optical constant (n and k) values of amorphous silicon (a-Si, 75 nm). Also shown for comparison existing data from literature[8], which shows a good match with our measurements.

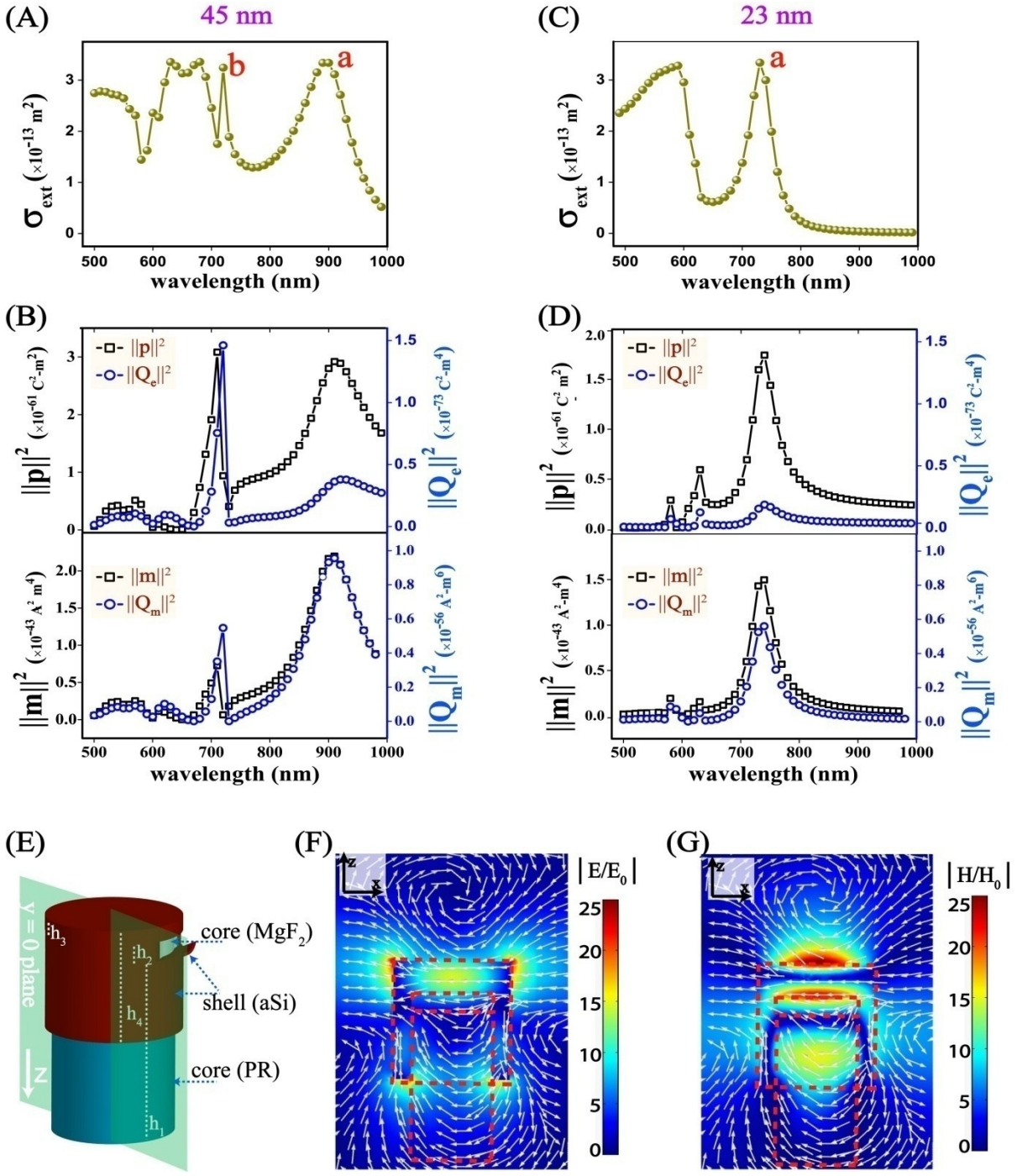

Figure S7: (A) Simulated extinction spectra for a 45 nm shell thickness PR-aSi core shell for normally incident light. (B) Plot of square of norm of dipole (electric, **p** and magnetic, **m**) and quadrupole (electric, $\mathbf{Q_e}$ and magnetic, $\mathbf{Q_m}$) moments (calculated through multipole decomposition) as a function of wavelength corresponding to 45 nm shell thickness. The resonance mode marked as 'a' in (A), though has contributions from **p**, $\mathbf{Q_e}$, $\mathbf{Q_m}$, is mainly dominated by **m** (as confirmed by the near field plots in Figure 1D of the main manuscript) while the mode marked as 'b' is dominated by $\mathbf{Q_e}$ (as confirmed by the near field plot shown in (F) and (G) below). (C) same as (A) but for 23 nm shell thickness. (D) same as (B) but for 23 nm shell thickness. Here also the resonance mode marked as 'a' in (C) is dominated by **m** (as confirmed by the near field plots in Figure 1D of the main manuscript). (E) Schematic of the model core shell system used in the simulation showing zx plane. (F) False colour plot of the norm of electric field enhancement ($|\mathbf{E/E_0}|$) at zx plane for PR-aSi core shell nanopillar with 45 nm shell thickness corresponding to the resonance dip marked as 'b' in (A). Arrows (white

colour) indicate direction of E vector in zx plane showing the typical electric quadrupole behaviour. (G) Same as (F) but for norm of magnetic field enhancement ($|\mathbf{H}/\mathbf{H_0}|$).

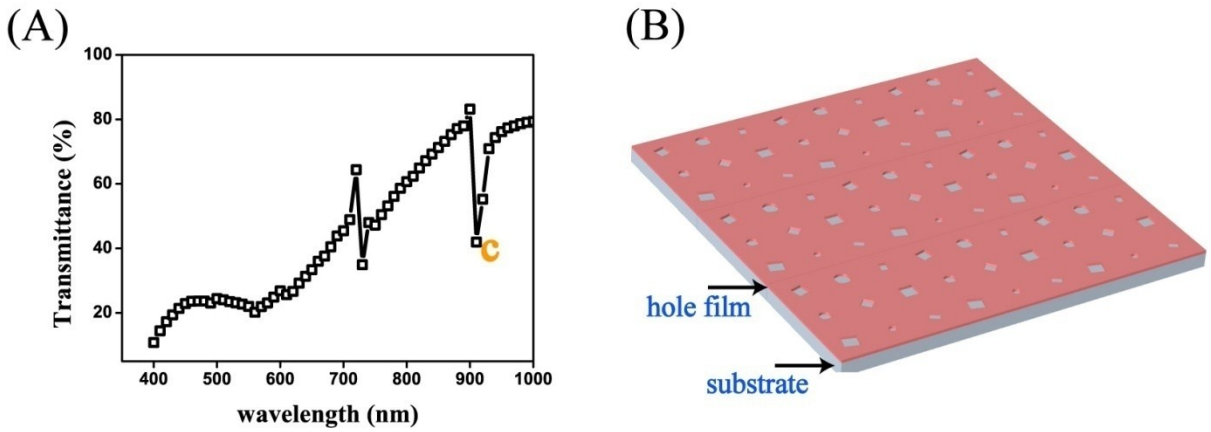

Figure S8: (A) Simulated transmittance spectra for aSi- hole array system corresponding to 38 nm film (aSi) thickness (B) Schematic of the hole array model system used in the simulation (irregularities in the hole shape and sizes are included). The location of the resonance 'c' is slightly different from that of the experiment shown in Fig 4B of the main manuscript which may be related to our inability to simulate the exact experimental system and the resonance of such a system is a strong function of the shape, size and depth of the holes as well as the array periodicity.

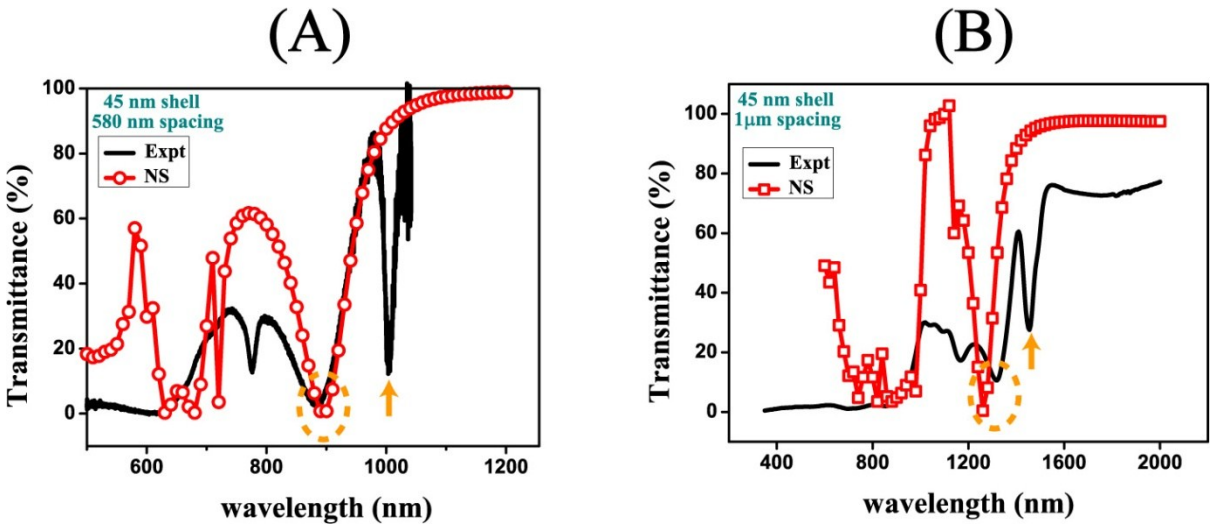

Figure S9: Measured (Expt) and Simulated (NS) transmittance spectra for a 45 nm shell thickness PR-aSi core shell nanopillar with (A) 580 nm and (B) 1 μm interpillar spacing. Core diameters for the two interpillar spacings are different (as it is difficult to fabricate two nanopillar array systems with same diameter but different array period with LIL). For 580 nm spacing the core diameter is around 200 nm and for 1 μm, diameter is around 450 nm. The spectra shift in the near-mid IR region for the 1 μm spacing is both due to change in interpillar spacing as well as core diameter. The spectral dips marked by arrows (seen only in the measured response) originates from the hole array like film deposited at the base of the substrate as discussed in the main manuscript.

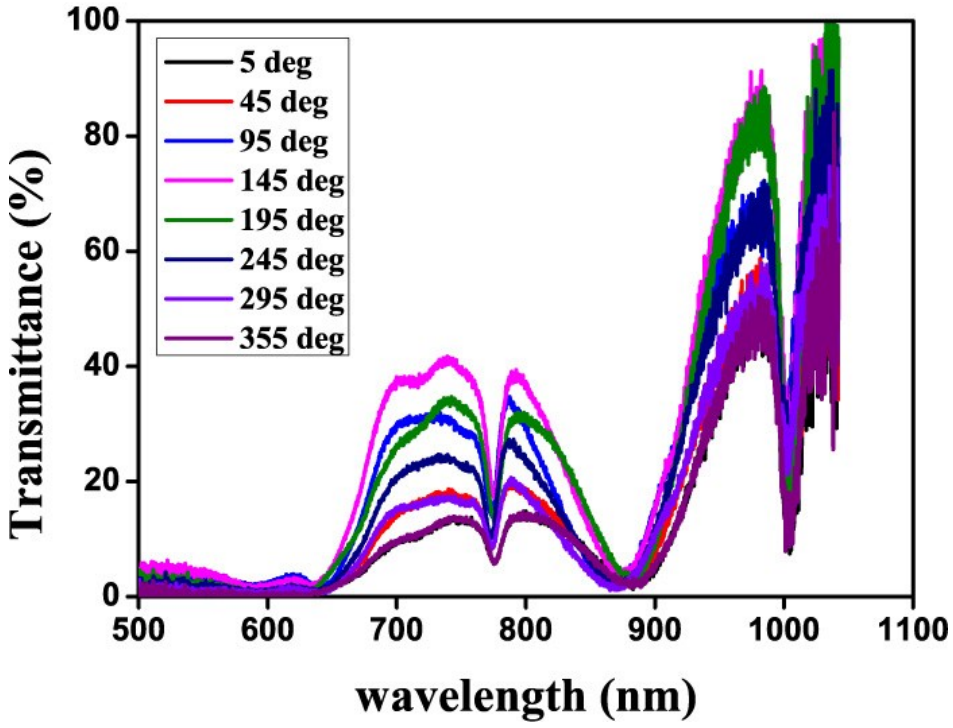

Figure S10: Measured transmittance spectra of a PR-aSi core shell nanopillar (45 nm shell thickness) for normally incident light as a function of direction of in plane polarization direction.

References:

1. S. Brueck, *Proceedings of the IEEE*, 2005, **93**, 1704-1721.
2. M. M. Hawkeye and M. J. Brett, *Journal of Vacuum Science & Technology A: Vacuum, Surfaces, and Films*, 2007, **25**, 1317-1335.
3. L. Martinu and D. Poitras, *Journal of Vacuum Science & Technology A: Vacuum, Surfaces, and Films*, 2000, **18**, 2619-2645.
4. C. Multiphysics, *COMSOL Multiphysics: a finite element analysis, solver and simulation software for various physics and engineering application, especially coupled phenomena, or multiphysics. URL http://www. comsol. com*.
5. R. Paniagua-Domínguez, Y. F. Yu, A. E. Miroshnichenko, L. A. Krivitsky, Y. H. Fu, V. Valuckas, L. Gonzaga, Y. T. Toh, A. Y. S. Kay and B. Luk'yanchuk, *Nature communications*, 2016, **7**, 10362.
6. E. Radescu and G. Vaman, *Physical Review E*, 2002, **65**, 046609.
7. F. Shafiei, F. Monticone, K. Q. Le, X.-X. Liu, T. Hartsfield, A. Alù and X. Li, *Nature nanotechnology*, 2013, **8**, 95.
8. D. Pierce and W. E. Spicer, *Physical Review B*, 1972, **5**, 3017.